

# Verification of moist surface variables over northern Australia in a high-resolution reanalysis (BARRA)

Peter T. May <sup>A,D</sup>, Blair Trewin <sup>B</sup>, Chun-Hsu Su <sup>B</sup> and Bertram Ostendorf <sup>C</sup>

<sup>A</sup>School of Earth Atmosphere and Environment, Monash University, Clayton, Australia.

<sup>B</sup>Bureau of Meteorology, Melbourne, Australia.

<sup>C</sup>University of Adelaide, Adelaide, Australia.

<sup>D</sup>Corresponding author. Email: [peter.may@monash.edu](mailto:peter.may@monash.edu)

**Abstract.** Reanalyses are important tools for understanding past weather and climate variability, but detailed verification of near surface humidity variables have not been published. This is particularly concerning in tropical regions where humid conditions impact meteorology and human activities. In this study, we used screen level temperature and humidity data from a high-resolution atmospheric regional reanalysis, the Bureau of Meteorology Atmospheric high-resolution Regional Reanalysis for Australia (BARRA), validated against automatic weather stations (AWS) data for 32 sites across northern Australia. Overall, the BARRA data was reliable, with the time series from the AWS and BARRA being very highly correlated, but there were some seasonal and diurnally varying biases. The variability of the differences also changed from location to location and as a function of time of day and season, but much less than the biases. This variability was less than the ‘weather signal’ as evidenced by the high correlations. In particular, the amplitude of the diurnal cycle was overestimated, particularly in the dry (winter) season. In general, the differences in temperature were larger than those of the dew point temperature, and the wet bulb temperature had the least uncertainty. Overall, this study contributes to a better understanding of the effectiveness of reanalyses for examining the impact of moist variables on tropical climate variability.

**Keywords:** BARRA, BARRA-R, high-resolution reanalysis, humidity, northern Australia, verification, wet bulb temperature.

Received 13 April 2021, accepted 6 August 2021, published online 20 September 2021

## 1 Introduction

Reanalyses are key tools in understanding past weather and climate trends over recent decades to a century. These have been used on global scales at modest spatial resolution (e.g. ~30–70 km) and at higher resolution on regional scales (~2–12 km). As expected, these reanalyses have been extensively verified against observational data, including surface and tower measurements of temperature and rainfall (e.g. Bosilovich *et al.* 2008; Decker *et al.* 2012; Su *et al.* 2019) as well as soundings (e.g. Jakobson *et al.* 2012). Other analyses have focussed on particular regions (e.g. Szczypka *et al.* 2011; Jakobson *et al.* 2012). Less attention has been paid to moist thermodynamic variables, such as the dew point temperature ( $T_D$ ) and wet bulb temperatures ( $T_{WB}$ ) near the surface, with some exceptions, such as comparison with column precipitable water (Bock *et al.* 2005). Nor has there been a focus on the tropics where the impact of humidity on meteorology and human activities are acute.

Given the difficulty of maintaining high quality wet bulb instrumental records (e.g. Lucas 2010), extremes of  $T_{WB}$  and

their trends are probably best explored through reanalyses. However, this requires an assessment of the accuracy of these analyses.

This study explores comparisons of hourly point surface observations with a 12-km atmospheric regional reanalysis data (Bureau of Meteorology Atmospheric high-resolution Regional Reanalysis for Australia, BARRA-R, or BARRA for brevity in this work; Su *et al.* 2019) at several sites in tropical northern Australia to explore this issue. Perfect agreement is not expected as local terrain and unresolved or poorly resolved local circulations may produce significant differences.

## 2 Data sets

Surface automatic weather station (AWS) data from the Australian Bureau of Meteorology has been collected from 32 sites in northern tropical Australia (Fig. 1, Appendix 1). These provide a wide geographic spread, with locations ranging from near coastal and peninsula sites to far inland. These sites record

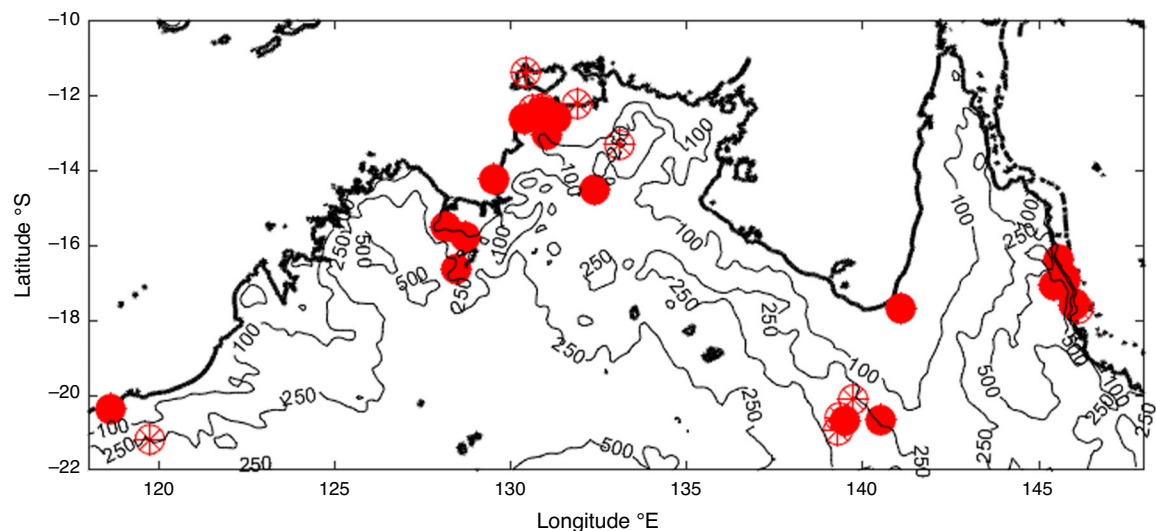


**Fig. 1.** Map showing AWS locations for this comparison. The solid circles represent those sites with records of 14 years or longer for the analysis of diurnal and seasonal variations comparison, and the shorter-record sites are shown as wheels. Contours from the BARRA topology data set are shown at 100, 250 and 500 m elevation.

hourly temperature ( $T$ ), relative humidity ( $RH$ ) and, in some locations,  $T_D$  and  $T_{WB}$ . Where  $T_{WB}$  was not recorded, it was calculated from the temperature and  $RH$  using the approximation of Stull (2011) given in Appendix 2. Likewise,  $T_D$  was calculated from the temperature and  $RH$  where it was not recorded. The Bureau of Meteorology AWS network is well supported, but there is occasional bad humidity data where the wet bulb sensors become dry and  $T \sim T_D \sim T_{WB}$ , but this only affects  $\sim 0.004\%$  of the data. The overlap of AWS data with the BARRA data set varies in length from less than a year to essentially the full data set with a median length of 13 years, but 13 of the sites are less than about 6 years long. There are 16 sites with records greater than 14 years.

The BARRA data is hourly, covers the period from January 1990 to February 2019 and has a horizontal grid spacing of around 12 km across Southeast Asia and the Maritime Continent as well as northern Australia. The data set comprises standard variables, including temperature, pressure, humidity, wind, cloud cover and rainfall. It was developed by assimilating a wide range of surface, satellite, aircraft and radiosonde observations in a coupled atmosphere–land model, namely the UK Met Office Unified Model for the atmosphere and the Joint UK Land Environment Simulator for the land (Walters *et al.* 2017). The model is set up with global atmosphere configurations suited for this moderate resolution and is nested within the European Centre for Medium-Range Weather Forecasts (ECMWF) Re-Analysis (ERA-Interim) global data set (Dee *et al.* 2011). BARRA is documented by Su *et al.* (2019).

Calculation of  $RH$  from the model data was performed using the approximations of Buck (1981), given in Appendix 2, for calculating saturation vapour pressure. Note this is very close to the Goff-Gratch formulation used in the modelling scheme for the warm temperatures in these regions. As with the observations, the  $T_{WB}$  was also calculated using the method of Stull (2011).

It should be noted that the observations used in the evaluation have also been assimilated in BARRA. Although the observational data is not strictly independent from BARRA, the data is a small part of an extensive range of observational data jointly assimilated in BARRA, and a significant part (50%) of the evaluated BARRA data sits outside the analysis windows (Su *et al.* 2019).

Since the BARRA grid is relatively coarse compared with the point observation footprint, there is always a height discrepancy between the grid cell height and the station altitude. This can be up to several hundred metres in mountainous terrain as can be found near parts of the Australian east coast. The bias from these height offsets is corrected by assuming a dry adiabat for all the temperature variables and constant specific humidity. Note this is strictly not correct, particularly near the surface, but it is a reasonable approximation over several hundred metres, and where the height difference is small, the correction is likewise small. This correction does act to reduce the bias in all cases, so is worthwhile.

### 3 Overall statistics

Data from the AWS and the BARRA analysis were matched in time, and the nearest land pixel was used. Note that some sites are on peninsulas and that the BARRA grid has some sites where the nearest grid point, such as Darwin airport, is characterised as an ocean grid point. The BARRA analyses show a rapid transition between off-shore and coastal locations of the surface temperature and humidity fields in terms of the diurnal cycle of temperature and the corresponding maximum and minimum temperatures ( $T_{\max}$  and  $T_{\min}$ , respectively) as has been observed near Darwin (e.g. May *et al.* 2012).

Time series for each site were collected, and the bias, standard deviation, skewness and correlation of the differences in  $T$ ,  $T_{WB}$  and  $RH$  between the AWS and BARRA data over the full station

data length were calculated. From these statistics we then computed the median bias and standard deviations in the distributions over all the sites for the overall statistics (Appendix 1), noting the record lengths at the various sites vary from one site as short as 6 months to the full 29 years with a median of 13 years (Appendix 1). No attempt was made to weight the results to those sites with longer records because we wanted to sample as many locations as possible, and as can be seen in Table 1, the range of values for each variable was relatively small. The skewness of the distributions were also relatively small.

The biases were much less than the standard deviations of the differences between the measurements. The magnitudes of the standard deviation of the temperature estimate differences were significant but generally much smaller than the daily and seasonal variations of the data, indicating that they were within a useful range for many applications. Note that the differences are at least partly due to comparing point measurements with an areal average and the corresponding lack of perfect overlap.

The correlations between the two estimates were very high for all the variables. This reflects a good mapping of the diurnal cycle and seasonal variations on both sets of time series, so high correlations are expected, but even the specific humidity shows correlations of order 0.9. Further, these high correlations mean that the covarying signal was much greater than the differences between the AWS and BARRA estimates even with the seasonal cycle removed.

The  $T_{WB}$  differences were systematically smaller than the temperature. The dynamic range of the individual  $T_{WB}$  time series tends to be smaller than the temperature, but notably, the variance was still less and correlations were higher despite the relative reduction in amplitude of the true variations and potential contributions from both the temperature and humidity terms.

#### 4 Statistics of daily maxima and minima

For many applications, it is the daily maximum and minimum values that are important. In order to test BARRA for this, in Table 2, we calculated the daily maxima and minima using a daily definition of 00–23 UTC to allow for the three time zones. With the daily cycle subtracted, the standard deviation of the differences between the AWS and BARRA was reduced, and the correlations remained very high, although there was some greater variance between sites. The bias values include the median bias over all the separate sites as well as the standard deviation of these biases. The variation between sites was comparable to or larger than the overall median bias. For all sites the magnitude of the average differences between the AWS and BARRA was less than the standard deviation of the differences.

However, the magnitude of the temperature biases was larger for these daily values than for the hourly time series, with BARRA showing a negative bias for the minimum temperature and positive for the maximum. Thus, BARRA overestimated the amplitude of the diurnal cycle of temperature at most sites over land, with a mean bias of 1.3°C. Su *et al.* (2019) compared the BARRA reanalysis with a semi-independent 5-km gridded surface analysis of temperature (and rainfall), Australian Water Availability Project (Jones *et al.* 2009). This comparison showed that BARRA underestimated the diurnal range over much of southern Australia, but gave more structure in the relatively sparsely observed northern area. In particular, the regions where our sites were used often showed similar overestimation of the diurnal cycle (Su *et al.* 2019, their Fig. 5). Note that overestimation of the amplitude of diurnal temperatures has also been reported in the ECMWF reanalysis for the Mississippi river basin (Betts *et al.* 2008). In contrast, the

**Table 1.** Median bias and standard deviation (s.d.) of the difference and correlation ( $\rho$ ) between the AWS data and the BARRA reanalysis (BARRA–AWS) over the 32 AWS. The biases in temperature were corrected for the height difference between the BARRA grid point and the AWS location assuming a dry adiabat and constant specific humidity

Variable/measure	Median bias	s.d. of differences	Median $\rho$	$\rho$ with seasonal cycle removed
T (°C)	$-0.2 \pm 0.6$	$2.2 \pm 0.5$	$0.91 \pm 0.03$	$0.88 \pm 0.03$
$T_{WB}$ (°C)	$-0.6 \pm 0.5$	$1.5 \pm 0.3$	$0.94 \pm 0.02$	$0.85 \pm 0.04$
$T_D$ (°C)	$-0.9 \pm 0.7$	$2.5 \pm 0.7$	$0.93 \pm 0.03$	$0.85 \pm 0.06$
RH (%)	$0 \pm 3$	$12 \pm 2$	$0.87 \pm 0.04$	$0.84 \pm 0.04$

**Table 2.** Median bias (BARRA–AWS), standard deviation (s.d.) and correlations of the two estimates of daily  $T_{max}$  and  $T_{min}$  values,  $T_D$  and  $T_{WB}$ . Again, the bias calculation includes height corrections as per the text

Variable/measure	Bias	s.d. of differences	Median $\rho$
$T_{max}$ (°C)	$0.8 \pm 0.6$	$1.6 \pm 0.5$	$0.91 \pm 0.13$
$T_{min}$ (°C)	$-0.7 \pm 1.2$	$1.7 \pm 0.4$	$0.94 \pm 0.03$
$T_{WB max}$ (°C)	$-0.8 \pm 0.5$	$1.0 \pm 0.5$	$0.95 \pm 0.05$
$T_{WB min}$ (°C)	$-0.5 \pm 0.8$	$1.6 \pm 0.4$	$0.96 \pm 0.02$
$T_D max$ (°C)	$-0.4 \pm 0.7$	$1.7 \pm 0.8$	$0.95 \pm 0.03$
$T_D min$ (°C)	$-0.8 \pm 0.9$	$2.5 \pm 0.7$	$0.94 \pm 0.02$

$T_{WB}$  and  $T_D$  biases were both cool (dry) and the diurnal variation only had a small bias. Note also the extremely high correlations between the two  $T_{WB}$  time series, reflecting the model data resolving the seasonal cycle but with relatively low noise.

The origin of these biases could arise from a number of sources, including local circulations, biases in surface, cloud, radiation and boundary layer parameterisations and the extrapolation from model level to the screen level. For example, AWS sites separated by only a few kilometres may have marked variations in minimum temperature associated with local circulations and drainage flows (e.g. Trewin 2005). Fig. 2 shows the mean biases and standard deviations of the temperature, dew point and wet bulb as a function of local time for those (16) sites with records greater than 14 years. All the temperature biases show similar behaviour with a rapid transition to BARRA being positively biased near sunrise and a more gradual shift to negative biases at sunset. In contrast, the average standard deviations of the differences show little diurnal cycle, but there are some sites where there are significant variations. In particular, there was an outlying curve from Argyle Aerodrome, located near a large inland lake, which showed a distinct

increase in the evening. The subgrid characterisation of the associated model grid cell includes this lake as inland water, but local circulations may still have an impact. Other sites showed some additional variations around sunrise and sunset, possibly arising from comparing points with areal averages. The  $T_D$  shows a negative (dry) bias in BARRA at all times, but this is larger during the day, possibly indicating too much mixing. The wet bulb bias sees the individual temperature and the dew point biases essentially cancel, albeit with an underestimation by BARRA with a minimum shortly after sunrise. The standard deviations of these moist variables show relatively small variance, although the  $T_{WB}$  differences tend to have smaller variability during the day.

The spatial distribution of these biases could provide some insights into their causes. Some of the largest  $T_{max}$  biases are near the coast, but these have nearby sites with small biases, so that the observed ocean–coastal transition of the temperature and humidity diurnal variations does not seem to be a major factor leading to errors (Fig. 3). Similar large variations in nearby sites are also seen inland. Likewise, the largest  $T_{min}$  biases tend to be inland, but again there is no clear spatial

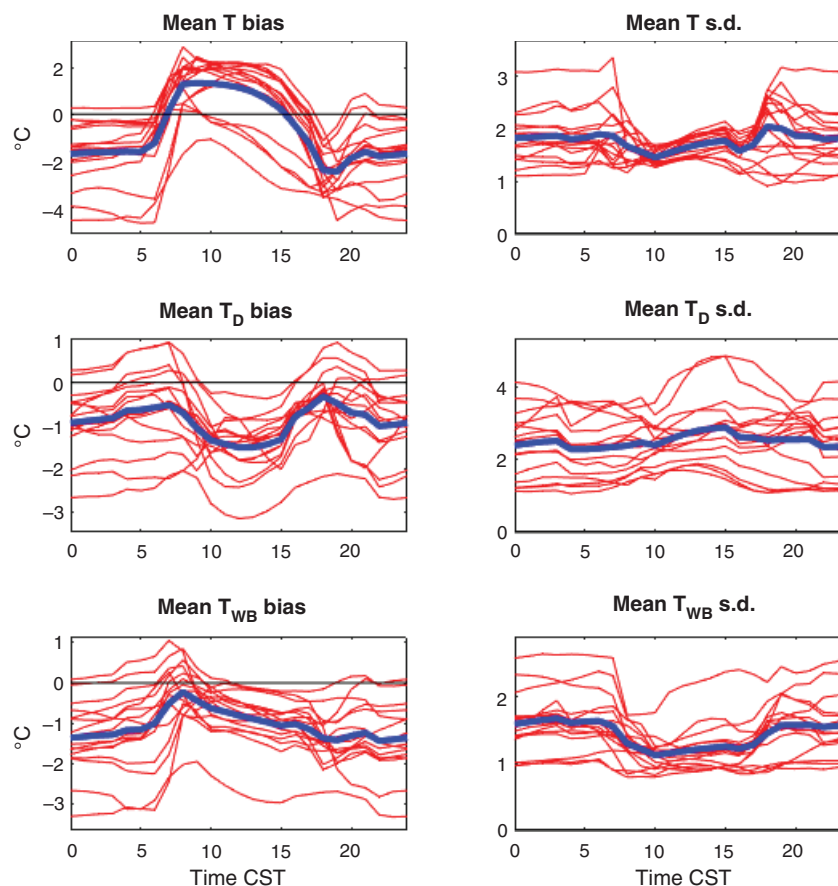


**Fig. 2.** Plots showing the mean bias and standard deviation (s.d.) of the BARRA-AWS temperature measurements as a function of local time of day (CST, UTC + 9:30) for a subset of 16 sites with records longer than 14 years. The red curves are for individual locations and the blue is the mean. CST is used as a standard here. Note the local times for some locations can differ by up to 90 min.

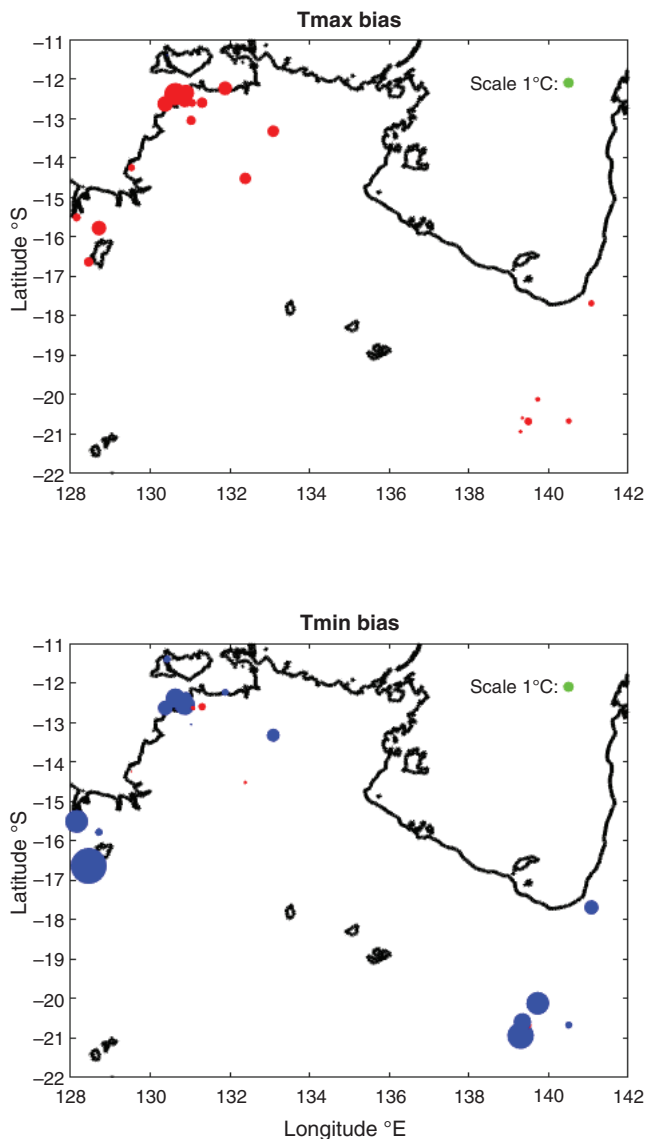


**Fig. 3.** Map of a subset of the sites showing the spatial distribution of the biases in  $T_{\max}$  and  $T_{\min}$ . A circle is drawn at each AWS site and the bias is proportional to the diameter of the circle. A  $1^{\circ}\text{C}$  reference is given in green. Positive (BARRA > AWS) biases are in red and negative are in blue.

patterns, with nearby sites exhibiting large variations in the bias, both near the coast and inland. Thus, there is also little evidence of systematic differences between the coastal areas and inland. This indicates that small-scale variability is important, with potentially unresolved circulations and their impacts as well as variations in land surface perhaps dominating other factors, such as radiation and the extrapolation, down to the 2 m level where biases may be expected to be more spatially uniform. The maxima and minima of  $T_D$  and  $T_{WB}$  also show small spatial scale variability and no clear signal. However, when these are combined, there is a clear north south gradient in the magnitude of the biases in the diurnal variation of the moist variables  $T_D$  and

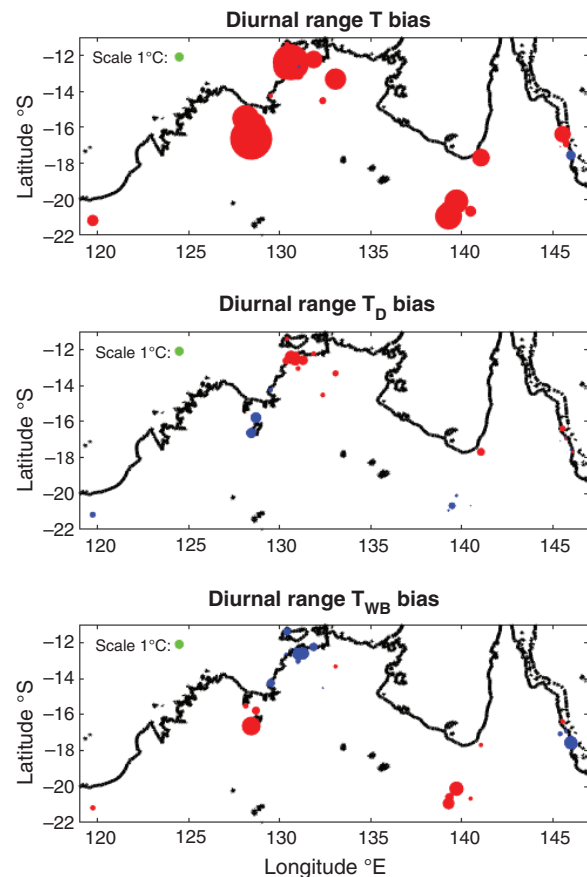


**Fig. 4.** Maps showing the amplitude of the bias in the diurnal range of  $T$ ,  $T_D$  and  $T_{WB}$ . A circle is drawn at each AWS site, and the bias is proportional to the diameter of the circle. A  $1^{\circ}\text{C}$  reference is given in green. Positive biases (BARRA > AWS) are in red and negative are in blue.

$T_{WB}$  (Fig. 4). Although this is a large spatial scale variation, it also reflects the meridional gradient of rainfall and soil moisture.

## 5 Seasonal variations

The diurnal variations of bias and potential linkages to the model boundary layer parameterisation, land surface and radiation schemes leads to the question of any systematic variations with season. Fig. 5 shows the seasonal variations for the mean bias and standard deviations of  $T$ ,  $T_D$  and  $T_{WB}$  for the same 16 locations. It is clear that the seasonal variations are much smaller than the diurnal ones, but there are still clear signals. There are significant variations between the various sites for all the variables, but the temporal variations are generally consistent. The temperature bias tends to be small and negative (AWS > BARRA) in the late winter and build-up (October–December) seasons whereas the variability slightly increases. These biases are smallest in the wet season (January–March) when there is the most convection, cloud cover, etc. (e.g. May *et al.* 2012 and references within). The  $T_D$  analyses show a dry bias in BARRA throughout the dry season (April–September), and this manifests as a consistent dry bias in the  $T_{WB}$ . The fact that these biases are smallest in the wet season indicates that



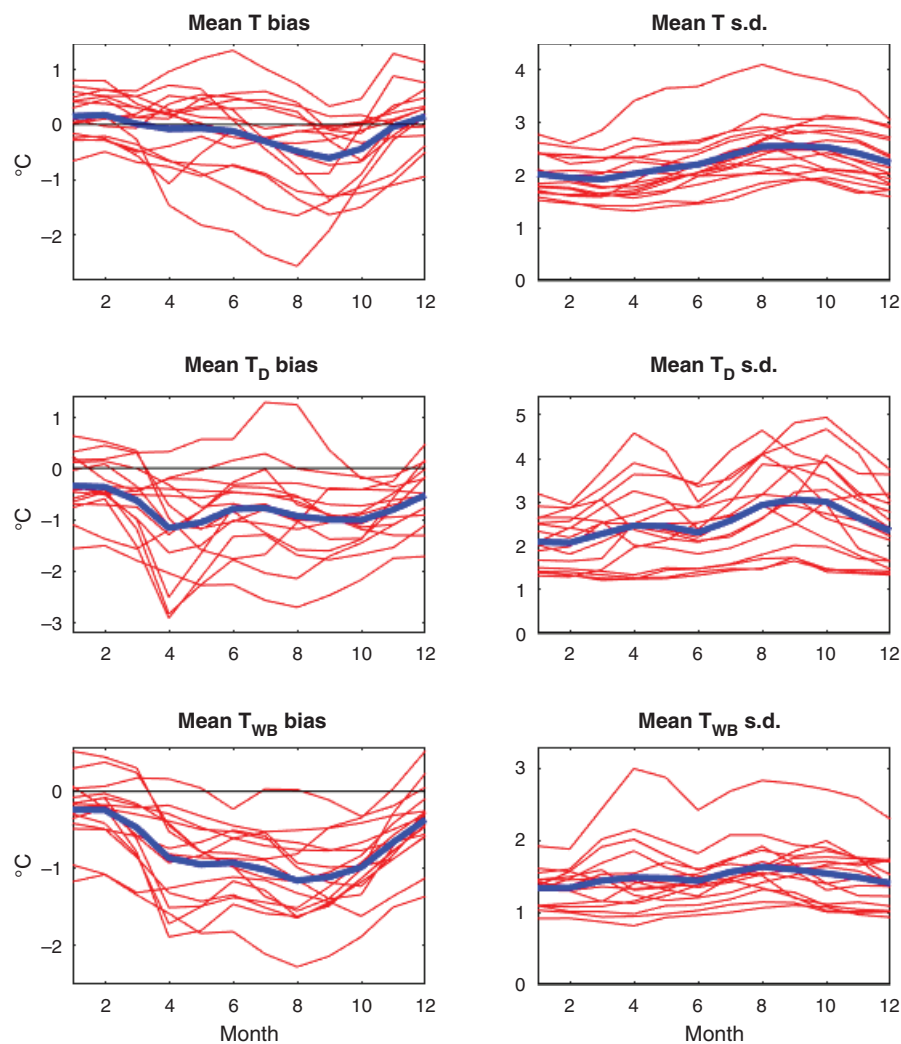


**Fig. 5.** Plots showing the mean bias and standard deviations of the BARRA–AWS temperature measurements as a function of season for a subset of 16 sites with records longer than 14 years. The red curves are for individual locations and the blue curve is the mean over all sites.

rainfall biases in BARRA (Su *et al.* 2019, section 3) are unlikely to be responsible for the overall dry bias. Similar to the diurnal biases, there was little consistent spatial structure evident in the sparse network when these biases were plotted on maps (not shown). There is far less seasonal variation in the standard deviations of the differences between the AWS and BARRA, although there is a weak maximum of the standard deviation of the differences in temperature and dew point in September and October, which is the end of the dry season.

We further expand on this by examining the biases and variation of the daily maxima and minima as a function of month (Fig. 6). The temperature panel shows a distinct cycle where the biases are relatively small in the wet season and progressively grow larger, with BARRA being greater than the AWS for  $T_{\max}$  and lower for  $T_{\min}$ . A candidate to explain this may be local flows. For example, as the amount of local convection increases in the build-up months prior to the monsoon a source of cool minimum

bias is where the AWS data may be affected by storm outflows associated with thunderstorms causing local temperature changes of several degrees, which will not be resolved in the reanalysis (e.g. Keenan and Carbone 1992; May 1999). However, the nighttime cool bias starts to increase well before the storm season, and the daytime warm bias also increases from mid-year until well into the build-up season. This points to some issues in the analysis in clear sky conditions for the screen level estimates. This could be associated with model biases in radiation, land surface characteristics and boundary layer parameterisations or the extrapolation from the lowest model level to the screen level. All may contribute.

The moisture variable ( $T_D$ ), in contrast, demonstrates a weaker seasonal variation of dry bias, but there is a clear increase in variability during the pre-monsoon build-up where local circulation trigger storms. Again, moist outflows may contribute to this, but the temperature variations do not show a

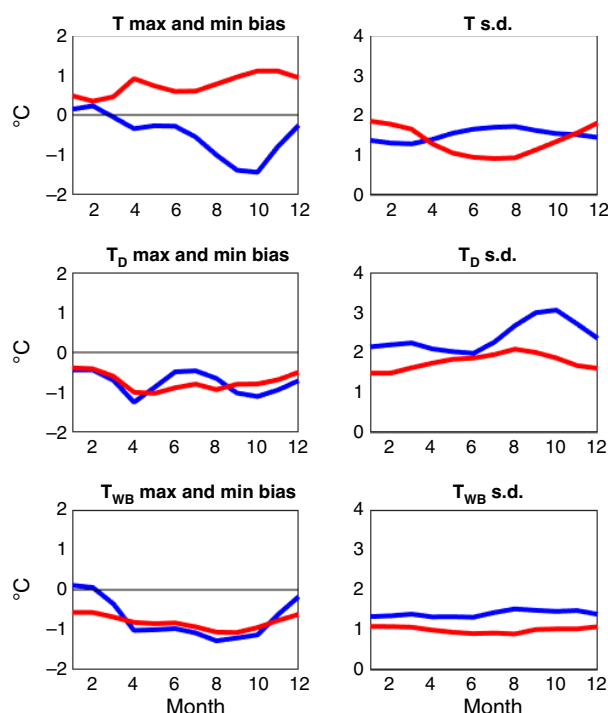


**Fig. 6.** Plots of the bias and standard deviations of difference between BARRA and the AWS stations estimated daily  $T_{\max}$  (red) and  $T_{\min}$  (blue),  $T_D$  and  $T_{WB}$  as a function of month for the stations with long records as per Fig. 5.

similar peak. These  $T$  and  $T_D$  variations result in low seasonal variability of  $T_{WB}$ .

## 6 Summary and conclusions

This paper compared the BARRA reanalysis temperature and humidity related screen level data with AWS data for a number of locations across northern Australia. This is particularly important for tropical regions, as the weather and its impact are affected by high humidity and measuring variables, such as  $T_{WB}$ , are prone to instrumental issues. We have focussed on the air temperature, the  $T_D$ , which is a purely humidity based variable, and the  $T_{WB}$ , which is a combination of temperature and humidity.

In general, there was good agreement between the AWS and BARRA time series considering the comparison is between areal averages and point measurements. The model biases relative to the observations and the standard deviation of those differences are generally less than the variability associated with weather systems, diurnal and seasonal variability, which gives confidence in their application. This is supported by the high correlations between the time series for all variables. There are seasonal variations in the daily  $T_{\max}$  and  $T_{\min}$  and generally smaller variations in the moist variables.

There were, however, some significant issues. In particular, the diurnal cycle of temperature was overestimated, and there were clear seasonal dependencies on both the mean biases and the seasonal variation of bias, with the dry season being most

affected. Bush *et al.* (2020) reported that the diurnal cycle representation in the Unified Model can be improved through various changes, including land cover characterisation, scalar roughness lengths for grass tiles and revisions to the albedos of vegetation tiles, and these changes could influence seasonal changes in the bias. The small-scale variations in the biases at different sites also indicates the importance of small-scale circulations and land surface variability. There were more modest variations in the standard deviations of maxima and minima of the temperature, etc., but there remain some significant seasonal variations. There was also evidence that some of these differences may be associated with local circulations induced by convection that are not resolved in the 12-km reanalysis as well as model limitations. It should be noted that future higher resolution reanalyses will reduce the issue of unresolved circulations.

## Data availability

The Bureau of Meteorology 2019 BARRA data set is available via the NCI Data Catalogue, Canberra (<http://dx.doi.org/10.4225/41/5993927b50f53>) The automatic weather station data used in this study is available on request or are available from the Bureau of Meteorology's climate database (<http://www.bom.gov.au/climate/data/>).

## Conflicts of interest

The authors declare no conflicts of interest.

## Declaration of funding

This research did not receive any specific funding.

## Acknowledgements

BARRA is produced by the Bureau of Meteorology in collaboration with Australian emergency service agencies and research institutions. We would also like to thank Peter Steinle, Yimin Ma and two anonymous reviewers for insightful reviews that significantly improved the paper.

## References

- Betts, A. K., Köhler, M., and Zhang, Y. (2008). Comparison of river basin hydrometeorology in ERA-Interim and ERA-40 with observations. ECMWF Tech. Memo. 568, 18 pp. doi:10.1029/2008JD010761
- Bock, O., Keil, C., Richard, E., Flamant, C., and Boen, M.-N. (2005). Validation of precipitable water from ECMWF model analyses with GPS and radiosonde data during the MAP SOP. *Quart. J. Roy. Meteor. Soc.* **131**, 3013–3036. doi:10.1256/QJ.05.27
- Bosilovich, M. G., Chen, J., Robertson, F. R., and Adler, R. F. (2008). Evaluation of global precipitation in reanalysis. *J. Appl. Meteor. Climatol.* **47**, 2279–2299. doi:10.1175/2008JAMC1921.1
- Buck, A. (1981). New equations for computing vapor pressure and enhancement factor. *J. Appl. Meteor.* **20**, 1527–1552. doi:10.1175/1520-0450(1981)020<1527:NEFCVP>2.0.CO;2
- Bush, M., Allen, T., Bain, C., Boutle, I., Edwards, J., Finnenkoetter, A., Franklin, C., Hanley, K., Lean, H., Lock, A., Manners, J., Mittermaier, M., Morcrette, C., North, R., Petch, J., Short, C., Vosper, S., Walters, D., Webster, S., Weeks, M., Wilkinson, J., Wood, N., and Zerroukat, M. (2020). The first Met Office Unified Model–JULES Regional Atmosphere and Land configuration, RAL1. *Geosci. Model Dev.* **13**, 1999–2029. doi:10.5194/GMD-13-1999-2020

- Decker, M., Brunke, M. A., Wang, Z., Sakaguchi, K., Zeng, X., and Bosilovich, M. G. (2012). Evaluation of the reanalysis products from GSFC, NCEP and ECMWF using flux tower observations. *J. Clim.* **25**, 1916–1944. doi:[10.1175/JCLI-D-11-00004.1](https://doi.org/10.1175/JCLI-D-11-00004.1)
- Dee, D. P., Uppala, S. M., Simmons, A. J., Berrisford, P., Poli, P., Kobayashi, S., Andrae, U., Balmaseda, M. A., Balsamo, G., Bauer, P., Bechtold, P., Beljaars, A. C. M., van de Berg, L., Bidlot, J., Bormann, N., Delsol, C., Dragani, R., Fuentes, M., Geer, A. J., Haimberger, L., Healy, S. B., Hersbach, H., Holm, E. V., Isaksen, I., Kallberg, P., Kohler, M., Matricardi, M., McNally, A. P., Monge-Sanz, B. M., Morcrette, J. J., Park, B. K., Peubey, C., de Rosnay, P., Tavolato, C., Thepaut, J. N., and Vitart, F. (2011). The Era-Interim reanalysis: Configuration and performance of the data assimilation system. *Quart. J. Roy. Meteor. Soc.* **137**, 553–597. doi:[10.1002/QJ.828](https://doi.org/10.1002/QJ.828)
- Jakobson, E., Vihma, T., Palo, T., Jakobson, L., Keernik, H., and Jaagus, J. (2012). Validation of atmospheric reanalyses over the central Arctic Ocean. *Geophys. Res. Lett.* **39**, L10802. doi:[10.1029/2012GL051591](https://doi.org/10.1029/2012GL051591)
- Jones, D. A., Wang, W., and Fawcett, R. (2009). High-quality spatial climate data-sets for Australia. *Aust. Meteorol. Oceanogr. J.* **58**, 233–248. doi:[10.22499/2.5804.003](https://doi.org/10.22499/2.5804.003)
- Keenan, T. D., and Carbone, R. E. (1992). A preliminary morphology of precipitation systems in tropical Northern Australia. *Quart. J. Roy. Meteor. Soc.* **118**, 283–326. doi:[10.1002/QJ.49711850406](https://doi.org/10.1002/QJ.49711850406)
- Lucas, C. (2010). A High-quality Historical Humidity Database for Australia, CAWCR Research Report 24, Bureau of Meteorology, ISBN 9781921605864 (pdf)
- May, P. T. (1999). Thermodynamic and vertical velocity structure of two gust fronts observed with a wind profiler/RASS during MCTEX. *Mon. Wea. Rev.* **127**, 1796–1807. doi:[10.1175/1520-0493\(1999\)127<1796:TAVVSO>2.0.CO;2](https://doi.org/10.1175/1520-0493(1999)127<1796:TAVVSO>2.0.CO;2)
- May, P. T., Protat, A., and Long, C. (2012). The diurnal cycle of the boundary layer, convection, clouds, and surface radiation in a coastal monsoon environment (Darwin Australia). *J. Clim.* **25**, 5309–5326. doi:[10.1175/JCLI-D-11-00538.1](https://doi.org/10.1175/JCLI-D-11-00538.1)
- Stull, R. (2011). Wet-bulb temperature from relative humidity and air temperature. *J. Appl. Meteor. Climatol.* **50**, 2265–2269. doi:[10.1175/JAMC-D-11-0143.1](https://doi.org/10.1175/JAMC-D-11-0143.1)
- Su, C.-H., Eizenberg, N., Steinle, P., Jakob, D., Fox-Hughes, P., White, C. J., Rennie, S., Franklin, C., Dharssi, I., and Zhu, H. (2019). BARRA v1.0: the Bureau of Meteorology Atmospheric high-resolution Regional Reanalysis for Australia. *Geosci. Model Dev.* **12**, 2049–2068. doi:[10.5194/GMD-12-2049-2019](https://doi.org/10.5194/GMD-12-2049-2019)
- Szczypta, C., Calvet, J.-C., Albergel, C., Balsamo, G., Boussetta, S., Carrer, D., Lafont, S., and Meurey, C. (2011). Verification of the new ECMWF ERA-Interim reanalysis over France. *Hydrol. Earth Syst. Sci.* **15**, 647–666. doi:[10.5194/HESS-15-647-2011](https://doi.org/10.5194/HESS-15-647-2011)
- Trewin, B. (2005). A notable frost hollow at Coonabarabran, New South Wales. *Aust. Met. Mag.* **54**, 15–21.
- Walters, D., Boutle, I., Brooks, M., Melvin, T., Stratton, R., Vosper, S., Wells, H., Williams, K., Wood, N., Allen, T., Bushell, A., Copsey, D., Earnshaw, P., Edwards, J., Gross, M., Hardiman, S., Harris, C., Heming, J., Klingaman, N., Levine, R., Manners, J., Martin, G., Milton, S., Mittermaier, M., Morcrette, C., Riddick, T., Roberts, M., Sanchez, C., Selwood, P., Stirling, A., Smith, C., Suri, D., Tennant, W., Vidale, P. L., Wilkinson, J., Willett, M., Woolnough, S., and Xavier, P. (2017). The Met Office Unified Model Global Atmosphere 6.0/6.1 and JULES Global Land 6.0/6.1 configurations. *Geosci. Model Dev.* **10**, 1487–1520. doi:[10.5194/GMD-10-1487-2017](https://doi.org/10.5194/GMD-10-1487-2017)



## Appendix 1.

A total of 32 AWS sites were selected. The record length ranges from 6 months up to the full BARRA record with a median length of 13 years.

**Table A1. AWS sites for reanalysis**

Site name	Latitude (°S)	Longitude (°E)	Station altitude (m)	BARRA grid point altitude	Record length (years)
Batchelor Airport	13.0544	131.0252	104	83	22
Channel Island	12.5557	130.8644	10	17	0.5
Charles Point	12.3895	130.6306	15	16	6
Darwin Airport	12.4239	130.8925	30	8	28
Dum in Mirrie Airstrip	12.635	130.3725	3	9	14
Lee Point	12.3582	130.8932	24	8	1
Middle Point	12.605	131.2988	14	20	16
Noonamah Airstrip	12.6099	131.0474	18	21	4.6
Noonamah AWS	12.6365	131.0714	27	21	4.5
Pirlangimpi Airport	11.4021	130.4217	18	15	11.
Point Stuart	12.2397	131.8791	1	2	5
Port Keats	14.2494	129.5282	28	8	15
South Johnstone Exp Stn	17.6053	145.9972	18	141	18
Cairns Aero	16.8736	145.7458	2	203	27
Cairns Racecourse	16.9463	145.7474	4	303	4.5
Cowley Beach	17.6905	146.1126	4	36	1
Low Isles Lighthouse	16.3842	145.5592	3	254	19
Mareeba	17.0704	145.4293	472	662	17
Innisfail Airport	17.5581	146.0119	12	57	1.6
Carters Bore	20.9358	139.2964	396	353	3.5
Cloncurry Airport	20.6664	140.505	186	206	17
Mt Isa Aero	20.6778	139.4875	340	406	22
New May Downs	20.59	139.3411	392	378	4.5
Lake Julius	20.1167	139.7256	237	273	4.5
Tindal RAAF	14.5229	132.3826	134	158	26
Central Arnhem Plateau	13.3275	133.0861	416	383	3
Marble Bar	21.1756	119.7497	182	247	11
Port Hedland Airport	20.3725	118.6317	6	16	22
Argyle Airport	16.638	128.4516	164	226	22
Kununurra Aero	15.7814	128.71	44	105	23
Wyndham Aero	15.51	128.15	4	86	17
Normanton Airport	17.6872	141.0733	18	11	17

## Appendix 2.

This paper uses the empirical fit of [Stull \(2011\)](#) to calculate wet bulb temperature,  $T_{WB}$ , from relative humidity, RH (%), and temperature,  $T$  (°C). The equation is:

$$T_{WB} = T \operatorname{atan} \left[ 0.151977(RH + 8.313659)^{1/2} \right] + \operatorname{atan}(T + RH) - \operatorname{atan}(RH - 1.676331) + 0.00391838(RH)^{3/2} \operatorname{atan}(0.023101RH) - 4.686035$$

The saturation vapour pressure (hPa) over liquid water,  $P_s(T)$ , calculation uses [Buck \(1981\)](#), which is more accurate than the Goff-Gratch formulation over the temperatures of interest.  $P_s(T)$  is given by:

$$P_s(T) = 0.61121 \exp[(18.678 - T/234.5)(T/(257.14 + T))]$$